Stability of Colloidal Iron Oxide Nanoparticles on Titania and Silica Support

Krans, Nynke A.; Van Uunen, Dónal L.; Versluis, Caroline; Dugulan, Achim Iulian; Chai, Jiachun; Hofmann, Jan P.; Hensen, Emiel J.M.; Zečević, Jovana; De Jong, Krijn P.

DOI
10.1021/acs.chemmater.0c01352

Publication date
2020

Document Version
Final published version

Published in
Chemistry of Materials

CHEMISTRY OF MATERIALS

pubs.acs.org/cm

Article

Stability of Colloidal Iron Oxide Nanoparticles on Titania and Silica Support

Nynke A. Krans, Dónal L. van Uunen, Caroline Versluis, Achim Iulian Dugulan, Jiachun Chai, Jan P. Hofmann, Emiel J. M. Hensen, Jovana Zečević, and Krijn P. de Jong*

Cite This: *Chem. Mater.* 2020, 32, 5226–5235

Read Online

ACCESS | Metrics & More | Article Recommendations | Supporting Information

ABSTRACT: Using model catalysts with well-defined particle sizes and morphologies to elucidate questions regarding catalytic activity and stability has gained more interest, particularly utilizing colloidally prepared metal(oxide) particles. Here, colloidally synthesized iron oxide nanoparticles (Fe_xO_y-NPs, size ~7 nm) on either a titania (Fe_xO_y/TiO_2) or a silica (Fe_xO_y/SiO_2) support were studied. These model catalyst systems showed excellent activity in the Fischer–Tropsch to olefin (FTO) reaction at high pressure. However, the Fe_xO_y/TiO_2 catalyst deactivated more than the Fe_xO_y/SiO_2 catalyst. After analyzing the used catalysts, it was evident that the Fe_xO_y-NP on titania had grown to 48 nm, while the Fe_xO_y-NP on silica was still 7 nm in size. STEM-EDX revealed that the growth of Fe_xO_y/TiO_2 originated mainly from the hydrogen reduction step and only to a limited extent from catalysis. Quantitative STEM-EDX measurements indicated that at a reduction temperature of 350 °C, 80% of the initial iron had dispersed over and into the titania as iron species below imaging resolution. The Fe/Ti surface atomic ratios from XPS measurements indicated that the iron particles first spread over the support after a reduction temperature of 300 °C followed by iron oxide particle growth at 350 °C. Mössbauer spectroscopy showed that 70% of iron was present as Fe^{2+}, specifically as amorphous iron titanates ($FeTiO_3$), after reduction at 350 °C. The growth of iron nanoparticles on titania is hypothesized as an Ostwald ripening process where Fe^{2+} species diffuse over and through the titania support. Presynthesized nanoparticles on SiO_2 displayed structural stability, as only ~10% iron silicates were formed and particles kept the same size during in situ reduction, carburization, and FTO catalysis.

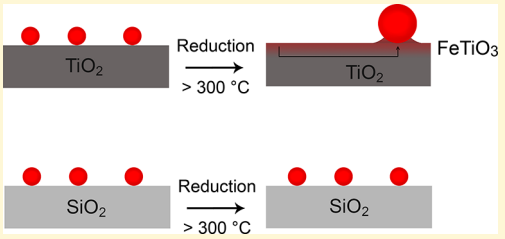

INTRODUCTION

Supported metal catalysts are of great importance in a wide range of catalytic processes.[1,2] The activity and selectivity of supported catalysts can be determined by the size, shape, and distribution of the active metal nanoparticles on the support, as well as metal–support interactions. As the catalytic reaction takes place on the surface of the metal nanoparticles, it is often the aim to obtain small particles, uniformly distributed on the support surface.[3] However, metal particles are typically prone to deactivation under industrially relevant conditions, prompting great efforts to design more stable catalysts.[4−7]

Many factors can contribute to catalyst deactivation, but a major cause is the loss of active metal surface area by nanoparticle growth.[8] In literature, two mechanisms are commonly used to describe the particle growth, namely, (i) Ostwald ripening and (ii) particle diffusion and coalescence. Mechanism i ensues due to the transport of atomic species diffusing from small nanoparticles to larger particles, via the support surface or gas/liquid medium. Depending on the metal, the diffusion of atomic species can be accelerated by reactive gasses such as H_2, CO, or H_2O.[9−13] Mechanism ii involves particle migration over the surface and coalescence to form larger particles. Different factors can affect the particle growth such as the initial particle size, particle-size distribution, and composition of the metal catalysts.[14] Furthermore, metal–support interactions have known to slow down or accelerate particle growth and can play a role in the particle growth mechanism.[15,16]

Strong interactions between the support and metal can influence the particle growth mechanisms.[17,18] Partial or complete encapsulation of metal nanoparticles by the support can occur when a reduced metal oxide is exposed to high-temperature treatments. In other cases, particles can be stabilized by the support due to the strong interaction, which may hinder the particle growth.[19,20] However, this effect can accelerate particle growth also, as atoms/ions from small metal nanoparticles can diffuse more easily over the support to form larger particles.[20] One of the supports prone to a strong interaction with metal nanoparticles is titania.

Titania is a reducible support and can go through several crystalline phases, namely, anatase, rutile, and brookite under

Received: March 30, 2020
Revised: May 27, 2020
Published: May 28, 2020

https://dx.doi.org/10.1021/acs.chemmater.0c01352
Chem. Mater. 2020, 32, 5226–5235

different reduction temperatures. Due to its reducibility, an extra challenge arises in the preparation of supported metal particles on titania. Until today, many studies have focused on elucidating the interactions between titania and metal particles such as Fe, Co, Rh, Ir, Ni, Pd, and Pt.[17,18,21−25] When the heat treatments necessary to create metal particles are performed, unreducible metal titanates can form.[24,26] This was found in the preparation for cobalt and iron on titania catalysts where often, during the reduction, cobalt and iron titanates form that cannot be reduced to the metallic state at typical reduction temperatures. When the metal oxide solid solutions cannot be converted into the active metallic iron phase, this causes deactivation of the catalyst.[27−29]

Iron and cobalt are used in Fischer−Tropsch catalysis, which involves the conversion of synthesis gas (CO/H_2) into hydrocarbon products. Depending on the catalyst used, the product selectivity can be tuned to either the formation of linear paraffins (cobalt-based catalysts) with high molecular weight or the production of olefins (iron-based catalysts), which is sometimes called Fischer−Tropsch-to-olefins (FTO).[26,30] Iron-based FTO catalysts are metal particle size, shape, and support sensitive.[31−33] Iron particles were previously supported on several materials such as carbon, silica, alumina, and titania where impregnation or coprecipitation is used as the synthesis method to prepare these catalysts. However, using an oxidic support such as silica, alumina, or titania can be challenging as nonreducible aluminates, silicates, and titanates can be formed during the heat treatment steps, restricting activation of the catalysts.[34−38]

An alternative synthesis method that separates the particle synthesis step from the attachment to the support is colloidal synthesis. Metal oxide particles can readily be made, and precursor solutions are not in contact with the metal oxide support. This means that the interaction of the metal particles with the support is substantially different compared to, e.g., impregnated or coprecipitated catalysts, because metal precursor contact with the support is avoided.[39−41] Using colloidal particles with the well-defined particle size, particle size distribution, shape, and composition can contribute to differentiate the catalyst properties that influence activity, selectivity, and stability.[42−44] In recent literature, colloidal synthesis methods were developed to synthesize iron oxide nanoparticles (Fe_xO_y-NPs) with great control over the size and shape. These Fe_xO_y-NPs can subsequently be attached to different support materials, with the objective to arrive at more stable catalysts.[33,45,46]

In this research, colloidal iron oxide nanoparticles were used to understand the growth of iron oxide supported on a silica or titania support. The colloidal iron oxide nanoparticles (Fe_xO_y-NPs) were synthesized with a narrow particle size distribution and average particle sizes of 7 nm. These Fe_xO_y-NPs were deposited on both a titania and silica support after which the well-distributed model catalysts were obtained (Fe_xO_y/SiO_2 and Fe_xO_y/TiO_2). The catalysts were subjected to FTO conditions where it was found that the particle size of the used Fe_xO_y/SiO_2 catalyst remained the same, whereas the iron oxide nanoparticles on the Fe_xO_y/TiO_2 catalyst had on average grown larger. This growth was further investigated for both catalysts using transmission electron microscopy (TEM) and scanning transmission electron microscopy (STEM) equipped with an energy-dispersive X-ray (STEM-EDX) detector for quantitative elemental mapping. Mössbauer, X-ray photoelectron spectroscopy (XPS), and temperature-programmed reduction (TPR) were used to obtain information about the iron species during or after hydrogen reduction. It was found that the reduction step caused the growth for Fe_xO_y/TiO_2 at temperatures above 300 °C. Instead, an Ostwald ripening mechanism was inferred where Fe^{2+} species diffuse over and through the titania support.

EXPERIMENTAL SECTION

Iron nanoparticles of approximately 7 nm were synthesized according to the procedure described by Casavola et al.[33] A 100 mL three-necked round bottom flask was filled with 1.2 mmol (0.35 g) hexadecanediol (≥ 98% purity), 0.75 mmol (0.21 g) oleylamine (70% purity), 0.43 g of oleic acid (90% purity), and 10 mL of 1-octadecene (90% purity). The flask was connected to a Schlenk line via a reflux condenser. The mixture was heated to 120 °C while stirring at 650 rpm with a glass-coated magnetic stirring bar. The flask was slowly brought to vacuum, and the mixture was degassed for 30 min. One millimole (0.21 g) iron pentacarbonyl ($Fe(CO)_5$) (99.99% purity) was weighed in a glovebox, and 1 mL of 1-octadecene was added. The three-necked round bottom flask was flushed three times with nitrogen gas and allowed to cool to 90 °C before injecting the $Fe(CO)_5$ solution into the heated mixture. The mixture was then heated to 290 °C with 10 °C/min. The temperature was maintained for 1 h to allow iron nanoparticle formation, and afterward, the obtained colloidal suspension was washed three times by adding five drops of toluene and a large excess of isopropanol followed by centrifugation (2700 rpm, 15 min). Lastly, the iron nanoparticles (Fe_xO_y-NPs) were dispersed in approximately 2 mL of toluene. (All chemicals were obtained from Sigma-Aldrich unless stated otherwise).

The Fe_xO_y-NPs were attached to a silica or titania support using a heating-up method.[33] A weight of 740 mg of the silica (Ox50 support Aerosil Evonik) or 800 mg of titania (P25 support Aeroxide Degussa Evonik) was placed in a three-necked round bottom flask, which was attached to a Schlenk line set-up via a reflux condenser. Ten milliliters of octadecene was mixed with the as-synthesized Fe_xO_y-NP dispersion, and the mixture was added to the support material while stirring at 400 rpm with a magnetic glass-coated stirring bar. To remove the toluene present in the Fe_xO_y-NP dispersion, the system was evacuated slowly while heating to 120 °C for half an hour. Next, the system was flushed three times with nitrogen gas and subsequently heated to 200 °C for 30 min. The mixture was allowed to cool to room temperature after which it was further processed in air. To remove all non-attached particles, the catalysts were washed six times with a hexane/acetone mixture (3: 1) followed by centrifugation (2700 rpm, 5 min). Subsequently, the catalysts were dried by a three-step drying method: at 60 °C in stagnant air for 1 h, at 120 °C in stagnant air for 3 h, and finally at 80 °C under vacuum for another 3 h. This three-step drying method was used to dry the catalysts and remove the organic ligands from the iron oxide particles as has been previously shown.[33] The Fe_xO_y-NP on titania will be referred to as Fe_xO_y/TiO_2, and the Fe_xO_y-NP on silica will be referred to as Fe_xO_y/SiO_2.

CHARACTERIZATION

Nitrogen-physisorption measurements were conducted at −196 °C using a Micromeritics Tristar 3000 to study the pore size and surface area of the support materials. The pore size distributions were determined from the adsorption branch of isotherms by the BJH method (between 1.7 and 300 nm). The total pore volume was taken as the single point pore volume at $P/P_0 = 0.995$.

X-ray diffraction (XRD) measurements were performed on a Bruker D2 phaser diffractometer with a fixed slit using Co Kα1 radiation with $\lambda = 1.78897$ Å. The measurements were taken at angles between 20 and 80 °2θ with an increment of 0.15 °2θ and a scan speed of 0.8−1 °2θ/s.

https://dx.doi.org/10.1021/acs.chemmater.0c01352
Chem. Mater. 2020, 32, 5226−5235

The elemental composition of the catalysts was determined by inductively coupled plasma atomic emission spectroscopy (ICP-AES) with a Thermo Jarrell Ash model ICAP 61E trace analyzer. The samples were prepared by an aqua regia extraction where the powdered sample (approximately 125 mg) was added to 1.5 mL of HNO_3 (65%) and 4.5 mL of HCl (30%) (1:3 ratio) in a destruction vessel and left overnight at 90 °C on a hot plate. The vessels were heated to 160 °C without caps until a gel was formed in less than 60 min. About 20 mL of (5%) HNO_3 was added to the vessels, closed, and subsequently heated to 90 °C overnight once more. Thereafter, the vessels were weighed to determine the dilution and measured to determine the iron content.

The catalysts were imaged using (scanning) transmission electron microscopy ((S)TEM). Sample (either Fe_xO_y-NP or Fe_xO_y/support) was dispersed in ethanol and drop-casted on 300 mesh copper grids with formvar (Fe_xO_y-NP) or the lacey carbon (Fe_xO_y/support) film. The samples were investigated using a Talos F200X (ThermoFisher Scientific) equipped with an X-FEG electron source operated at 200 kV. Energy-dispersive X-ray (EDX) maps were acquired using the same apparatus with a Super-XTM EDX detector in a STEM mode. Average particle sizes were determined by measuring around 300 metal nanoparticles per sample using ImageJ program.

To prepare the samples for (S)TEM, a droplet of dispersed Fe_xO_y/TiO_2 in ethanol was added onto a copper lacey grid. To determine the local and average iron loading of the supported catalysts, STEM-EDX spectra were collected from ~0.5 μm^2 areas of samples. The spectra were acquired using Velox software (FEI) with a 10-min acquisition time. Ten different spectra were used to calculate the average loading of the sample, while areas from these spectra revealed the local iron loading in the regions where no iron nanoparticles were observed. Spectrum background correction and the peak analysis were performed using the software-integrated methods.

In vacuo transfer XPS using a Kratos AXIS Ultra 600 spectrometer equipped with a monochromatic Al Kα X-ray source ($h\nu$(Al Kα) = 1486.6 eV) was employed to study the iron particle growth on the titania and silica supports. Survey scans were recorded at a pass energy of 160 eV (a step size of 0.5 eV) with the background pressure kept below 5×10^{-9} mbar.

A high-temperature reaction cell (Kratos, WX-530) was used to pretreat the sample, which was supported on an aluminum stub, allowing in vacuo sample transfer into the XPS measurement chamber. The reduction was performed in a 66% H_2 in Ar flow at atmospheric pressure at three reduction temperatures, viz., 240, 300, and 350 °C for 2 h with 5 °C/min. After reduction at each temperature, the sample was cooled down and subsequently transferred to the XPS analysis chamber in vacuo. Quantitative analysis was done by measuring the peak areas of specific elemental core lines (Fe2p, Si2p, and Ti2p) in the region scans and by applying appropriate atomic sensitivity factors.

Transmission ^{57}Fe Mössbauer spectra were collected at 120 K with a sinusoidal velocity spectrometer using a ^{57}Co(Rh) source. Velocity calibration was carried out using an α-Fe foil at room temperature. The source and the absorbing samples were kept at the same temperature during the measurements. The Mössbauer spectra were fitted using Mosswinn 4.0 program.[47] The experiments were performed in a state-of-the-art high-pressure Mössbauer in situ cell developed at Reactor Institute Delft.[48] The high-pressure beryllium windows used in this cell contain 0.08% iron impurity whose spectral contribution was fitted and removed from the final spectra. Reduction was carried out for 2 h at 240, 300, and 350 °C (H_2/Ar = 2, 1 bar), and after each temperature, a spectrum was obtained.

To investigate the reduction of the catalysts, temperature-programmed reduction (TPR) was performed. A weight of 25−50 mg of catalyst (75−150 μm sieve fraction) was reduced in a 15 mL/min H_2 gas flow while increasing the temperature with 5 °C/min ramp up to 900 °C. The off-gas was analyzed using a thermal conductivity detector (TCD), and certain components were analyzed using a mass spectrometer.

To investigate the effect of the reduction step, 10−20 mg of catalyst sieved to a grain size of 75−150 μm was mixed with 150−200 mg of SiC (212−450 μm sieve fraction) and transferred to a tubular glass reactor. The catalyst was then reduced in a flow of a 15 mL/min H2/Ar gas mixture (H_2/Ar = 2: 1 v/v) for 2 h at temperatures ranging from 240 to 350 °C. The temperatures were reached with a heating ramp of 5 °C/min. The GHSV during these experiments was ~10,000 h^{-1}. A CO reduction was performed with the same samples as described above. Fe_xO_y/TiO_2 was dried for 2 h at 350 °C before performing the reduction step to eliminate all residual water. The catalyst was then reduced in a flow of 15 mL/min CO/Ar gas mixture (CO/Ar = 2:1 v/v) for 2 h at 350 °C.

CATALYST PERFORMANCE

Fischer−Tropsch reactions were carried out using an Avantium Flowrence 16-port parallel fixed-bed reactor setup. Around 10−20 mg of catalyst sieved to a grain size of 75−150 μm was mixed with 200 mg of SiC (212−450 μm sieve fraction) and transferred to a stainless-steel reactor. The catalyst was then reduced in situ at 3 bar with a 103.3 mL/min H_2/He gas mixture (H_2/He = 1:2) for 2 h at 350 °C and carburized at 3 bar and 290 °C for 1 h with a 132 mL/min CO/H_2 gas mixture (a ratio of 2:1). Catalysis was performed for 100 h at 300 °C with GHSV = 72,600−103,700 h^{-1} and 2:1 CO/H_2 at 10 bar. All temperatures were preceded by a heating ramp of 5 °C/min.

RESULTS

Iron oxide nanoparticles (Fe_xO_y-NPs) were synthesized via a colloidal route and thereafter analyzed using transmission electron microscopy (TEM), see Figure 1A. The average particle size was 7 nm with a narrow size distribution (±1 nm),

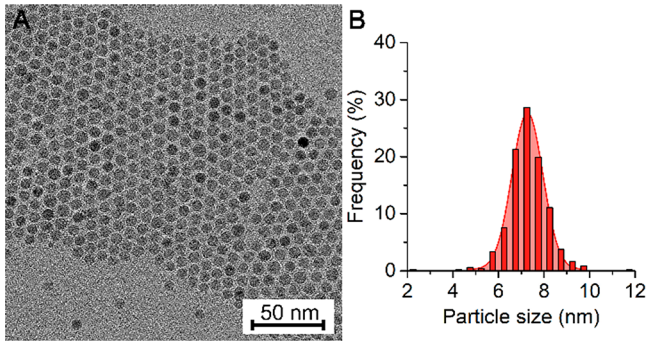

Figure 1. Colloidal iron oxide nanoparticles. (A) Transmission electron microscopy image of the colloidal particles dried on a TEM grid. (B) The histogram of the particle size distribution.

https://dx.doi.org/10.1021/acs.chemmater.0c01352
Chem. Mater. 2020, 32, 5226−5235

as can be seen from the histogram in Figure 1B. Particles dried on the TEM grid were separated by ~2 nm corresponding to the length of the organic ligands used in this synthesis method.[49,50]

The TiO_2 and SiO_2 supports were analyzed using nitrogen physisorption to obtain the BET surface area, see Table 1 and Figure S1 in the Supporting Information. Both materials had similar specific surface areas and a broad pore size distribution, with titania showing larger total pore volume and more (~25−75 nm) mesopores than silica.

Table 1. Surface Area of both Supports, Iron Oxide Particle Size, and Iron Weight Loading

sample name	support BET surface area (m^2/g)[a]	iron oxide particle size(nm)[b]	iron weight loading (wt %)[c]
Fe_xO_y/SiO_2	45	7.3 (±0.8)	3.3
Fe_xO_y/TiO_2	42	7.1 (±1.0)	2.9

[a]The BET surface area was determined by nitrogen physisorption at −196 °C. [b]Particle sizes were obtained by measuring ~300 particles from TEM images. [c]Iron weight loading was determined by ICP analysis.

Particles were attached to both support materials and analyzed using TEM. Samples were named Fe_xO_y/SiO_2 when attached to the silica support (Figure 2A) and Fe_xO_y/TiO_2 when attached to the titania support (Figure 2B). The Fe_xO_y-NPs were homogeneously attached to the silica support, while on the titania support, empty regions were observed also, revealing heterogeneities in particle distribution.

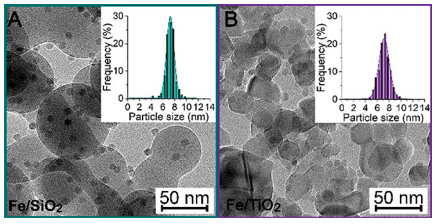

Figure 2. TEM micrographs of the attached iron oxide nanoparticles. (A) Particles attached to SiO_2 and (B) particles attached to TiO_2. The insets show the histograms of the particle sizes.

The inset histograms show that the Fe_xO_y-NP size distributions were similar for both catalysts and the as-synthesized Fe_xO_y-NPs in Figure 1. The average particle sizes of the Fe_xO_y-NPs and the iron weight loadings were determined by TEM and ICP, respectively, see Table 1. The weight loading of both catalysts was around 3 wt %, while the particle sizes remained 7 nm on average.

X-ray diffractograms were obtained for both catalysts and a blank for the TiO_2 support, see Figure 3. The iron on silica showed a broad peak around 24 °2θ originating from the amorphous silica[49] and also peaks, which correspond to the magnetite or maghemite phase of iron oxide. The iron on titania only showed peaks from two different titania phases (rutile and anatase, in line with the expectation of this titania material[50]). For this catalyst no iron oxide peaks could be identified, which is probably caused by the strong signal from the titania overlapping with the iron oxide peaks between 42 and 75 °2θ.

The performance of the two catalysts was investigated in the Fischer−Tropsch-to-olefin reaction in which both were

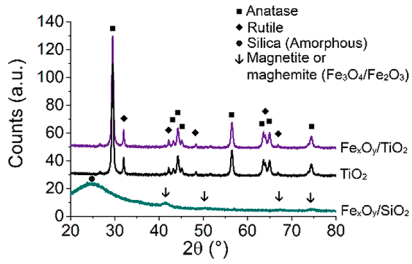

Figure 3. X-ray diffractograms of Fe_xO_y/SiO_2, blank TiO_2, and Fe_xO_y/TiO_2. The different phases identified in Fe_xO_y/TiO_2 are anatase (black square) and rutile (black diamond) (offsets of 30 counts for TiO_2 and 50 counts for Fe_xO_y/TiO_2), while for Fe_xO_y/SiO_2 amorphous silica (black circle) and Fe_3O_4 magnetite or γ-Fe_2O_3 maghemite (black arrow) were found.

subjected to syngas (CO/H_2 ratio of 2:1) at 10 bar for 100 h time on stream (TOS) after in situ reduction in H_2 and carburization in a mixture of H_2 and CO gas. The reduction was used to both reduce the iron oxide to metallic iron and remove any residual organic ligands on the surface of these particles.[6] The activity in iron time yield (FTY) was plotted against the time on stream (Figure 4A). Fe_xO_y/SiO_2 had a higher activity compared to Fe_xO_y/TiO_2. For Fe_xO_y/SiO_2, an activity decrease of 30% was found while Fe_xO_y/TiO_2 showed a 60% decrease after a 100 h time on stream. The selectivities (at time on stream (TOS) = 100 h) of both catalysts can be found in the Supporting Information, Table S1, and were comparable for both catalysts. Moreover, when an impregnated iron on the silica catalyst from previous literature is compared to the colloidally prepared catalysts in this research,[51] the colloidal model catalyst in present research showed higher activity (FTY) most probably due to the well-developed particles in the fresh catalysts.

The used catalysts were investigated using TEM. The Fe_xO_y/SiO_2 catalyst showed only little change after the catalytic reaction, with average Fe_xO_y-NP sizes of 7 nm and a standard deviation of ±0.9 nm, as can be seen in Figure 4B. The particle size distribution of the used silica-supported catalyst overlapped the distribution of the fresh catalyst almost perfectly (Figure 4C), indicating that the structural stability of this the iron nanoparticles on silica is impeccable. The 30% decrease in catalytic activity in Figure 4A was therefore not attributed to particle growth but most probably due to other contributing factors such as coke or iron silicate formation.[26] Surprisingly, the morphology of the Fe_xO_y/TiO_2 catalyst had dramatically changed after catalysis, as shown in Figure 4D,E. Fe_xO_y-NP could no longer be distinguished from TiO_2 particles in the TEM images (Figure 4D). An energy-dispersive X-ray (EDX) map shown as an overlay of a STEM image can be found in Figure 4E. Iron nanoparticles are indicated in red color and showed larger particles with an average size of 48 nm (±20 nm), see Figure 4F. As the decrease in catalytic activity could not be solely explained by the growth in particles, especially for the silica, the reduction pretreatment was investigated in more depth.

The reduction step of the catalysts was investigated at 1 bar. A temperature-programmed reduction measurement was done for both Fe_xO_y/TiO_2 and Fe_xO_y/SiO_2 (see Figure 5) under hydrogen from 200 to 450 °C with 5 °C/min. The reduction of both catalysts initiated around 275 °C where Fe_xO_y/SiO_2 showed a two-step reduction. The reduction behavior of the two catalysts is relatively similar to work done in previous

https://dx.doi.org/10.1021/acs.chemmater.0c01352
Chem. Mater. 2020, 32, 5226−5235

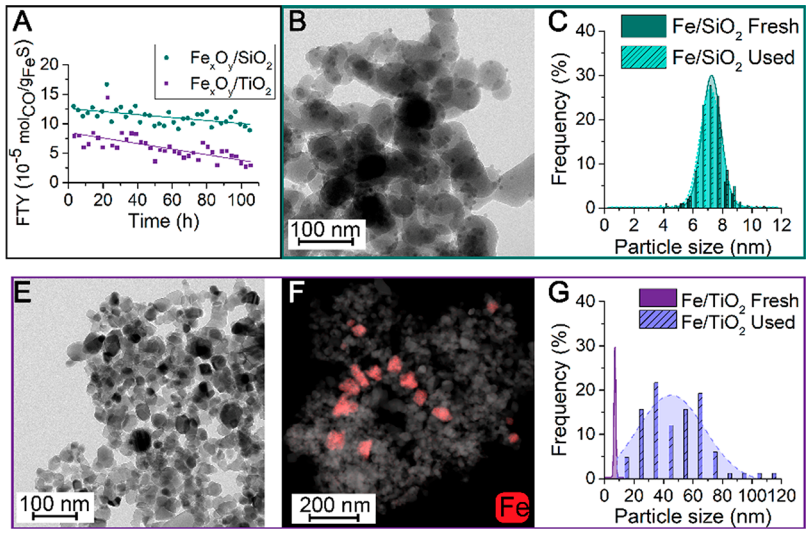

Figure 4. FTO catalysis results and TEM images of Fe_xO_y/SiO_2 and Fe_xO_y/TiO_2 after 100 h TOS under FTO conditions at 10 bar. (A) Catalytic activities shown as FTY (iron time yield) in mol CO converted per gram iron per second as a function of time-on-stream (TOS). (B) TEM image of the used Fe_xO_y/SiO_2 catalyst. (C) Particle size histogram of the fresh and used Fe_xO_y/SiO_2. (D) TEM image of the used Fe_xO_y/TiO_2 catalyst. (E) Scanning transmission electron microscope (STEM) image with an energy-disperse X-ray (EDX) map overlay of the used Fe_xO_y/TiO_2 catalyst showing the iron in red. (F) Particle size distribution of fresh and used Fe_xO_y/TiO_2.

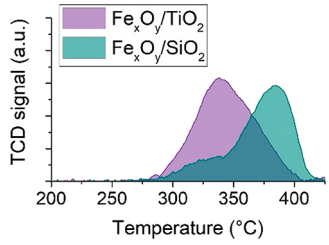

Figure 5. Temperature-programmed reduction experiments of iron oxide nanoparticles with a ramp of 5 °C/min up to 425 °C. In green, the TPR of Fe_xO_y/SiO_2, while in purple, the TPR of Fe_xO_y/TiO_2 is shown.

literature of iron on carbon supports.[41] The peak of the reduction in the TPR measurement displayed a shift toward lower temperatures for Fe_xO_y/TiO_2, which was consistent with previous literature as surface titanium ions can induce the reduction of surface Fe^{3+} species.[52]

To investigate the reduction step in more detail, STEM images with an EDX map (Figure 6) as an overlay of Fe_xO_y/TiO_2 after hydrogen reduction for 2 h at either 240, 275, 300, 325, or 350 °C are shown, with temperatures increasing from left to right, respectively. At reduction temperatures of 240, 275, and 300 °C, the average particle size remained 7 nm (Figure 6A–C), as also shown by the particle size distribution histograms in Figure 6F. Increasing the reduction temperature up to 325 °C resulted in a broader particle size distribution (Figure 6G) and a less homogeneous particle distribution on the titania support (Figure 6D). Moreover, TEM images (Figure S2 in the Supporting Information) revealed that the spherical iron oxide nanoparticles from the fresh catalysts had now changed to hemispherical particles, indicating a decreased

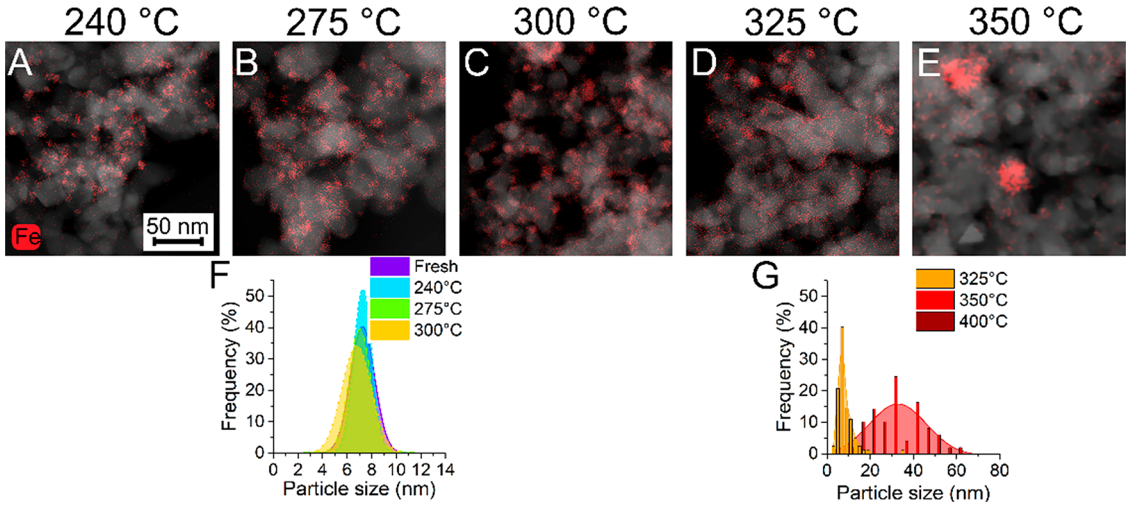

Figure 6. STEM images and particle size distributions of Fe_xO_y/TiO_2 after reduction using H_2/Ar for 2 h at different temperatures. (A–E) STEM images with EDX map overlay (iron in red) of reduction temperatures ranging from 240 °C (left) to 350 °C (right). (F) Fe_xO_y-NP size distributions after reduction temperatures 240, 275, and 300 °C. (G) Particle size distributions after reduction at 325 and 350 °C.

https://dx.doi.org/10.1021/acs.chemmater.0c01352
Chem. Mater. 2020, 32, 5226–5235

wetting angle with the titania surface, which indicates a strong interaction with the titania support.[20] Analyzing particles after a reduction of 2 h with a temperature of 350 °C, showed particles with an average of 40 nm in size and a broad particle size distribution (Figure 6E,G). The additional particle growth observed with the used catalysts (Figure 4F) could explain the decrease in catalytic activity shown in Figure 4A and originate from particle growth due to iron carbide formation as observed in previous research.[46] The iron particle sizes were close to the TiO_2 support particle size (~42 nm), making it difficult to distinguish iron particles from support particles using TEM as was also observed for Fe_xO_y/TiO_2 after FTO (Figure 4D).

EDX spectra were used to quantify the iron content on the support material in regions where no iron oxide nanoparticles were observed (for preparation details see the Experimental Section) for all the reduction temperatures mentioned above. In the EDX spectrum originating from Area 1 (Figure 7A),

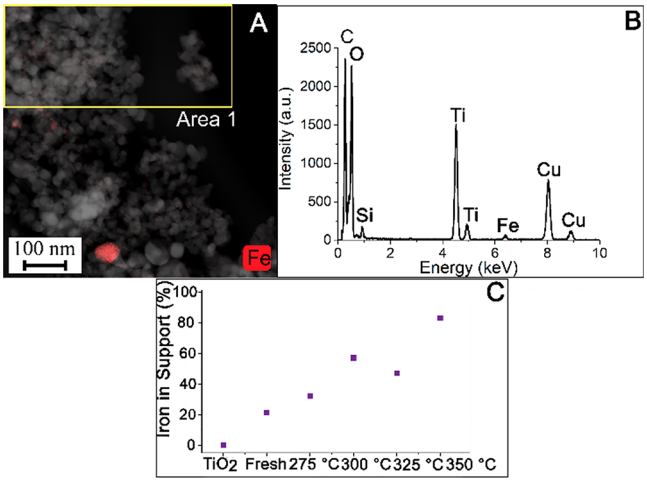

Figure 7. EDX measurements of Fe_xO_y/TiO_2. (A) An EDX overlay on a STEM-HAADF image indicating an area (Area 1) showing no iron oxide nanoparticles. (B) Carbon, oxygen, silicon, titanium, iron, and copper can be distinguished in the EDX spectrum from Area 1. Copper, carbon, and silicon originated from the copper lacey grid used to disperse the sample on. (C) The iron content in the particle-free support regions (w/w) is plotted for the bare TiO_2, fresh Fe_xO_y/TiO_2, and the reduced Fe_xO_y/TiO_2 samples at temperatures ranging from 275 to 350 °C.

copper, iron, titanium, carbon, oxygen, and silicon could be found where copper, carbon, and silicon were signals coming from the grid used for the preparation. In areas such as Area 1, an iron signal could clearly be distinguished (Figure 7B), indicating that the iron was present as dispersed species below imaging resolution. The iron content (w/w) of this given area (see Figure 7A) was measured and divided by the Fe content detected in the whole STEM-EDX image. This gave the iron content found in the support for the bare titania support, the fresh catalyst, and the reduced catalyst at different temperatures (Figure 7C). The bare titania support contained no iron, while the fresh catalyst already had 20% of the initial 2.9 wt % iron present in a highly dispersed form. Moreover, an increase of this iron content was found with increasing reduction temperature up to 80% at 350 °C, meaning that roughly 2.3 wt % iron was situated on the support in a highly dispersed form. Furthermore, at this temperature, no hemispherical particles were found anymore. This showed that the increase in reduction temperature increased the iron oxide wetting onto and reaction with the titania support. From Figures 6 and 7, it is concluded that the reduction step induced iron redistribution onto the support (~80% of iron present) with concomitant particle growth (~20% of iron present).

To investigate the influence of water formed during reduction with hydrogen,[5,13,53,54] the reduction of the Fe_xO_y/TiO_2 catalyst was performed with CO instead of H_2. The histogram in Figure S3A in the Supporting Information showed once more an increase in the average particle size (~24 nm) as well as a broad particle size distribution. The EDX map in Figure S3B revealed the larger particles, but also a low number of 7 nm particles was observed (indicated by the arrow in Figure S3A). Moreover, to assess the influence of heat treatment as such on the particle growth, the fresh catalyst was heated to 350 °C for 2 h in argon, see Figure S3C. The size histogram of the heat-treated catalyst overlapped the histogram of the fresh catalyst. As the particles still grew in a water-free environment and as the particle size stayed the same size during a heattreatment of 350 °C, this led to the conclusion that neither water nor heat was main parameter for the growth of the particles on titania but rather the reduction treatment.

XPS wide-scan spectra were measured of both catalysts after reduction with hydrogen at 240, 300, and 350 °C, see Figure S4 in the Supporting Information. Due to inelastic scattering within the samples, photoelectrons generated more than 2−5 nm below the surface do not contribute to the signal. Therefore, the surface atomic ratio of Fe/Si and Fe/Ti provide information about size and structure of supported iron phases.[55,56] For Fe_xO_y/SiO_2, it was found that the Fe/Si ratios stayed similar after the increase in reduction temperatures (Table 2) confirming that the iron particles were not altered as also observed from the TEM images (Figure 4B).

However, for Fe_xO_y/TiO_2, the Fe/Ti ratio did change with increasing reduction temperatures at an H_2 atmosphere, showing an increased ratio at 300 °C where after the ratio decreased again at 350 °C (Table 2). This increase in the Fe/Ti ratio indicated a higher dispersion of iron over the titania support during the reduction. We explain this by a strong interaction of iron and titania in comparison to iron and silica. After reduction at the highest temperature, the Fe/Ti ratio decreased; however, this is in qualitative agreement with the growth of particles shown by TEM (Figure 6E).

Mössbauer results were obtained for Fe_xO_y/TiO_2 and Fe_xO_y/SiO_2 to investigate the phase transitions of the iron species at the different reduction temperatures, which are shown in Figure S5 and Table S2 in the Supporting Information. The quadrupole splitting (QS) value in Table S2 (a measure of the charge asymmetry around the Fe atoms) can be used to identify the different iron phases and their dispersion on the surface of the catalysts at different reduction temperatures.[57] Fe_xO_y/SiO_2 showed a phase transition of Fe^{2+} and Fe^{3+} species toward Fe^{2+} and Fe^0 when reduced at higher temperatures (Table S2). FeO species were already found at 240 °C, indicating that at this temperature the iron oxide nanoparticles were partially reduced.[58] Furthermore, at a reduction temperature of 350 °C, 12% Fe^{2+} species were observed to interact strongly with the silica support, indicating that the loss in catalytic activity found in Figure 4A can be explained by a limited amount of formation of iron silicates. Upon reduction of the Fe_xO_y/TiO_2 catalyst, Fe^{2+} and Fe^{3+} species were found also, but the QS value of Fe^{2+} was higher, indicating that Fe^{2+} was strongly interacting with the titania

https://dx.doi.org/10.1021/acs.chemmater.0c01352
Chem. Mater. 2020, 32, 5226−5235

Table 2. X-ray Photoelectron Spectroscopy Results with Surface Atomic Ratios of Both Catalysts after Different Reduction Temperatures

Catalyst Support	Reduction Temperature (°C)	Fe/Si ratio (at/at) [a]	Schematic representation [b]	Catalyst Support	Fe/Ti ratio (at/at) [a]	Schematic representation [b]
SiO_2	240	0.06	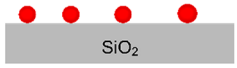	TiO_2	0.30	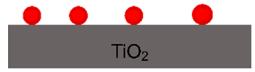
SiO_2	300	0.05	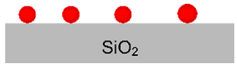	TiO_2	0.39	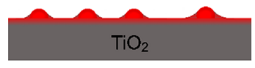
SiO_2	350	0.06	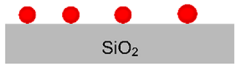	TiO_2	0.28	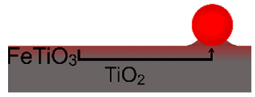

[a]Quantitative analysis was done by measuring the peak areas of the Fe2p, Si2p, and Ti2p core lines and by applying appropriate atomic sensitivity factors in the survey scans. The estimated error of the surface atomic ratios was ±0.01 at/at for Fe/Si and ± 0.03 at/at for Fe/Ti. [b]Schematic representations were based on XPS, STEM-EDX, TEM, and Mössbauer data.

support already at 240 °C.[59−62] This was observed in previous literature also, as iron and titania can relatively easily form iron titanate species.[54] The Fe^{2+} species for Fe_xO_y/TiO_2 had a QS distinctive for amorphous $FeTiO_3$ species,[63] which decreased when the reduction temperature was increased, indicating sintering of the iron into large iron (oxide) particles.[64]

TEM results indicated a spreading of 80% of the iron species onto the support as Fe^{2+}, and Mössbauer simultaneously showed a similar amount (70%) of amorphous $FeTiO_3$ with increasing reduction temperature. In addition, XPS showed that as the reduction temperature increases, the iron distributed onto the surface of the titania. For common growth mechanisms, particle growth is initiated by species moving over the support; however in this case, the iron is not situated on the support but has formed a new phase due to a strong interaction between the iron oxide and titania. Therefore, it is postulated that the growth of the iron particles occurred via an Ostwald ripening process, which involves Fe^{2+} species from smaller particles moving through the support to form larger particles (Table 2, last entry). The final particle size of the Fe_xO_y-NP (∼40 nm) after reduction at 350 °C is close to the pore size of the titania support (38 nm) and suggests growth of the iron oxide due to Ostwald Ripening in confinement, as earlier observed for example for nickel catalysts.[65]

In literature, it is often mentioned that iron silicates can form also, just as iron titanates, under a reducing atmosphere at elevated temperatures.[26,38] Therefore, it is remarkable that in this study the iron titanates induced growth, while the small amount of iron silicates that was seen in Mössbauer did not induce any growth. When using an impregnation method, a precursor solution of iron ions is in direct contact with the support, which may give rise to iron silicate formation[51] opposed to the use of colloids where the silica is in direct contact with preformed and distinct iron oxide nanoparticles. It is hypothesized that due to this difference in synthesis method, the colloidal attached particles are more stable, considering that it might be a slow process for solid iron oxide to react with in an unreducible support.

CONCLUSIONS

In this research, colloidally obtained iron oxide nanoparticle (Fe_xO_y-NP) model catalysts were synthesized and attached to either a silica support (Fe_xO_y/SiO_2) or a titania support (Fe_xO_y/TiO_2). During the Fischer−Tropsch-to-olefin reaction, both catalysts deactivated over time with Fe_xO_y/SiO_2 deactivating less than Fe_xO_y/TiO_2. When investigating the used catalysts, it was found that an initial particle size of 7 nm (±1 nm) did not change after catalysis for Fe_xO_y/SiO_2, indicating that the deactivation was most likely due to coke or a limited extent of iron silicate formation. However, the titania-supported iron oxide particles had grown from the initial 7 nm to much larger particles 48 nm with a broad size distribution of ±20 nm.

This significant difference in structural stability was most prominent upon reduction and further investigated using TPR, STEM-EDX imaging, and quantitative EDX measurements combined with information from Mössbauer and XPS. Interestingly, it appeared that during reduction temperatures >300 °C the iron oxide particles on average grew with the largest growth observed at 350 °C. STEM-EDX and TEM images showed only particles larger than 20 nm and dispersed iron species below imaging resolution. Fe/Ti surface atomic ratios from XPS indicated that dispersion/wetting of iron particles increased on the titania surface at 300 °C, and substantial iron particle growth took place at a temperature of 350 °C. Mössbauer spectroscopy showed that 70% of iron was in the Fe^{2+} form at 350 °C, with peaks of Fe^{2+} from amorphous $FeTiO_3$ species. These three observations suggest that an amorphous $FeTiO_3$ layer on the TiO_2 support was formed due to the strong interactions of TiO_2 with the iron oxide. The Fe^{2+} species on the titania support also gave rise to an Ostwald ripening mechanism where species move over and through the support during the reduction. For SiO_2, this was not the case, as this support is unreducible and did not easily form a mixed oxide support to a significant extent using presynthesized iron oxide particles. Finally, this study shows that, by separating the synthesis of the iron oxide nanoparticles from the attachment step, catalysts can be obtained, which are extremely helpful in enhancing structural stability and/or in revealing mechanisms of nanoparticle growth processes.

ASSOCIATED CONTENT

Supporting Information

The Supporting Information is available free of charge at https://pubs.acs.org/doi/10.1021/acs.chemmater.0c01352.

https://dx.doi.org/10.1021/acs.chemmater.0c01352
Chem. Mater. 2020, 32, 5226−5235

Nitrogen physisorption, TEM and STEM images, XPS spectra, and the extensive Mössbauer spectroscopy (PDF)

AUTHOR INFORMATION

Corresponding Author

Krijn P. de Jong − *Inorganic Chemistry and Catalysis, Debye Institute for Nanomaterials Science, Utrecht University, Utrecht 3584 CG, The Netherlands;* orcid.org/0000-0002-9773-8110; Email: k.p.dejong@uu.nl

Authors

Nynke A. Krans − *Inorganic Chemistry and Catalysis, Debye Institute for Nanomaterials Science, Utrecht University, Utrecht 3584 CG, The Netherlands;* orcid.org/0000-0002-3764-3187

Dónal L. van Uunen − *Inorganic Chemistry and Catalysis, Debye Institute for Nanomaterials Science, Utrecht University, Utrecht 3584 CG, The Netherlands*

Caroline Versluis − *Inorganic Chemistry and Catalysis, Debye Institute for Nanomaterials Science, Utrecht University, Utrecht 3584 CG, The Netherlands*

Achim Iulian Dugulan − *Fundamental Aspects of Materials and Energy Group, Delft University of Technology, Delft 2629 JB, The Netherlands*

Jiachun Chai − *Inorganic Materials and Catalysis, Department of Chemical Engineering and Chemistry, Eindhoven University of Technology, Eindhoven 5600 MB, The Netherlands*

Jan P. Hofmann − *Inorganic Materials and Catalysis, Department of Chemical Engineering and Chemistry, Eindhoven University of Technology, Eindhoven 5600 MB, The Netherlands;* orcid.org/0000-0002-5765-1096

Emiel J. M. Hensen − *Inorganic Materials and Catalysis, Department of Chemical Engineering and Chemistry, Eindhoven University of Technology, Eindhoven 5600 MB, The Netherlands;* orcid.org/0000-0002-9754-2417

Jovana Zečević − *Inorganic Chemistry and Catalysis, Debye Institute for Nanomaterials Science, Utrecht University, Utrecht 3584 CG, The Netherlands*

Complete contact information is available at: https://pubs.acs.org/10.1021/acs.chemmater.0c01352

Funding

We acknowledge the European Research Council, EU FP7 ERC advanced grant no. 338846. J.Z. acknowledges financial support by the Netherlands Organization for Scientific Research (NWO), Veni grant no. 722.015.010.

Notes

The authors declare no competing financial interest.

ACKNOWLEDGMENTS

Miguel Rivera Torrente is thanked for nitrogen physisorption measurements, and Coen Mulder is thanked for ICP-AES measurements.

ABBREVIATIONS

EDX, energy-dispersive X-ray spectroscopy; Fe_xO_y-NP, iron oxide nanoparticle; Fe_xO_y/TiO2, iron nanoparticles on titania support; Fe_xO_y/SiO2, iron nanoparticles on silica support; FTO, Fischer−Tropsch-to-olefins; FTY, iron time yield; ICP-AES, inductively coupled plasma atomic emission spectroscopy; TEM, transmission electron microscopy; TPR, temperature-programmed reduction; STEM, scanning transmission electron microscopy; XPS, X-ray photoelectron spectroscopy; XRD, X-ray diffraction.

REFERENCES

(1) White, R. J.; Luque, R.; Budarin, V. L.; Clark, J. H.; MacQuarrie, D. J. Supported Metal Nanoparticles on Porous Materials Methods and Applications. *Chem. Soc. Rev.* **2009**, *38*, 481−494.

(2) Aricò, A. S.; Bruce, P.; Scrosati, B.; Tarascon, J. M.; Van Schalkwijk, W. Nanostructured Materials for Advanced Energy Conversion and Storage Devices. *Nat. Mater.* **2005**, *4*, 366−377.

(3) Munnik, P.; De Jongh, P. E.; De Jong, K. P. Recent Developments in the Synthesis of Supported Catalysts. *Chem. Rev.* **2015**, *115*, 6687−6718.

(4) Campbell, C. T.; Parker, S. C.; Starr, D. E. The Effect of Size-Dependent Nanoparticle Energetics on Catalyst Sintering. *Science* **2002**, *298*, 811−814.

(5) Masoud, N.; Delannoy, L.; Schaink, H.; Van der Eerden, A.; De Rijk, J. W.; Silva, T. A. G.; Banerjee, D.; Meeldijk, J. D.; De Jong, K. P.; Louis, C.; De Jongh, P. E. Superior Stability of Au/SiO_2 Compared to Au/TiO_2 Catalysts for the Selective Hydrogenation of Butadiene. *ACS Catal.* **2017**, *7*, 5594−5603.

(6) Krans, N. A.; Weber, J. L.; Van den Bosch, W.; Zečević, J.; De Jongh, P. E.; De Jong, K. P. Influence of Promotion on the Growth of Anchored Colloidal Iron Oxide Nanoparticles during Synthesis Gas Conversion. *ACS Catal.* **2020**, *10*, 1913−1922.

(7) Prieto, G.; Zečević, J.; Friedrich, H.; De Jong, K. P.; De Jongh, P. E. Towards Stable Catalysts by Controlling Collective Properties of Supported Metal Nanoparticles. *Nat. Mater.* **2013**, *12*, 34−39.

(8) Xin, H. L.; Mundy, J. A.; Liu, Z.; Cabezas, R.; Hovden, R.; Kourkoutis, L. F.; Zhang, J.; Subramanian, N. P.; Makharia, R.; Wagner, F. T.; Muller, D. A. Atomic-Resolution Spectroscopic Imaging of Ensembles of Nanocatalyst Particles Across the Life of a Fuel Cell. *Nano Lett.* **2012**, *12*, 490−497.

(9) Hansen, T. W.; Delariva, A. T.; Challa, S. R.; Datye, A. K. Sintering of Catalytic Nanoparticles: Particle Migration or Ostwald Ripening? *Acc. Chem. Res.* **2013**, *46*, 1720−1730.

(10) Wynblatt, P.; Gjostein, N. A. Supported Metal Crystallites. *Prog. Solid State Chem.* **1975**, *9*, 21−58.

(11) Sadeqzadeh, M.; Hong, J.; Fongarland, P.; Curulla-Ferré, D.; Luck, F.; Bousquet, J.; Schweich, D.; Khodakov, A. Y. Mechanistic Modeling of Cobalt Based Catalyst Sintering in a Fixed Bed Reactor under Different Conditions of Fischer-Tropsch Synthesis. *Ind. Eng. Chem. Res.* **2012**, *51*, 11955−11964.

(12) Horch, S.; Lorensen, H. T.; Helveg, S.; Lægsgaard, E.; Stensgaard, I.; Jacobsen, K. W.; Nørskov, J. K.; Besenbacher, F. Enhancement of Surface Self-Diffusion of Platinum Atoms by Adsorbed Hydrogen. *Nature* **1999**, *398*, 134−136.

(13) Parkinson, G. S.; Novotny, Z.; Argentero, G.; Schmid, M.; Pavelec, J.; Kosak, R.; Blaha, P.; Diebold, U. Carbon Monoxide-Induced Adatom Sintering in a Pd-Fe_3O_4 Model Catalyst. *Nat. Mater.* **2013**, *12*, 724−728.

(14) Bartholomew, C. H.; Farrauto, R. J. *Fundamentals of Industrial Catalytic Processes*; John Wiley & Sons: Hoboken, New Jersey, 2006.

(15) Oschatz, M.; Hofmann, J. P.; Van Deelen, T. W.; Lamme, W. S.; Krans, N. A.; Hensen, E. J. M.; de Jong, K. P. Effects of the Functionalization of the Ordered Mesoporous Carbon Support Surface on Iron Catalysts for the Fischer−Tropsch Synthesis of Lower Olefins. *ChemCatChem* **2017**, *9*, 620−628.

(16) Van Deelen, T. W.; Hernández Mejía, C.; de Jong, K. P. Control of Metal-Support Interactions in Heterogeneous Catalysts to Enhance Activity and Selectivity. *Nat. Catal.* **2019**, *2*, 955−970.

(17) Tauster, S. J.; Fung, S. C.; Garten, R. L. Strong Metal-Support Interactions. Group 8 Noble Metals Supported on titanium dioxide. *J. Am. Chem. Soc.* **1978**, *100*, 170−175.

(18) Hernández Mejía, C.; Van Deelen, T. W.; De Jong, K. P. Activity Enhancement of Cobalt Catalysts by Tuning Metal-Support Interactions. *Nat. Commun.* **2018**, *9*, 4459.

(19) Moon, S. Y.; Naik, B.; Jung, C. H.; Qadir, K.; Park, J. Y. Tailoring Metal-Oxide Interfaces of Oxide-Encapsulated Pt/Silica Hybrid Nanocatalysts with Enhanced Thermal Stability. *Catal. Today* **2016**, *265*, 245−253.
(20) Pan, C. J.; Tsai, M. C.; Su, W. N.; Rick, J.; Akalework, N. G.; Agegnehu, A. K.; Cheng, S. Y.; Hwang, B. J. Tuning/Exploiting Strong Metal-Support Interaction (SMSI) in Heterogeneous Catalysis. *J. Taiwan Inst. Chem. Eng.* **2017**, *74*, 154−186.
(21) Bezemer, G. L.; Falke, U.; Van Dillen, A. J.; De Jong, K. P. Cobalt on Carbon Nanofiber Catalysts: Auspicious System for Study of Manganese Promotion in Fischer-Tropsch Catalysis. *Chem Commun.* **2005**, 731−733.
(22) Vannice, M. A.; Garten, R. L. Metal-Support Effects on the Activity and Selectivity of Ni Catalysts in CO/H_2 Synthesis Reactions. *J. Catal.* **1979**, *56*, 236−248.
(23) Santos, J.; Phillips, J.; Dumesic, J. A. Metal-Support Interactions between Iron and Titania for Catalysts Prepared by Thermal Decomposition of Iron Pentacarbonyl and by Impregnation. *J. Catal.* **1983**, *81*, 147−167.
(24) Fu, Q.; Wagner, T. Interaction of Nanostructured Metal Overlayers with Oxide Surfaces. *Surf. Sci. Rep.* **2007**, *62*, 431−498.
(25) Zhang, S.; Plessow, P. N.; Willis, J. J.; Dai, S.; Xu, M.; Graham, G. W.; Cargnello, M.; Abild-pedersen, F.; Pan, X. Dynamical Observation and Detailed Description of Catalysts under Strong Metal - Support Interaction. *Nano Lett.* **2016**, *16*, 4528−4534.
(26) Torres Galvis, H. M.; De Jong, K. P. Catalysts for Production of Lower Olefins from Synthesis Gas : A Review. *ACS Catal.* **2013**, *3*, 2130−2149.
(27) Boot, L. A.; Van der Linde, S. C.; Van Dillen, A. J.; Geus, J. W.; Van Buren, F. R.; Bongaarts, J. E. The Behavior of Titania-Supported Iron Oxide Catalysts in Butene Dehydrogenation. *Stud. Surf. Sci. Catal.* **1994**, *88*, 491−498.
(28) Fiato, R. A.; Kugler, E. L.; Gardner, G. Iron on Titania Fischer-Tropsch Catalyst, US Patent: 4,689,313, *August 25*, 1987.
(29) Rayner, M. K.; Billing, D. G.; Coville, N. J. In-Situ X-Ray Diffraction Activation Study on an Fe/TiO_2 Pre-Catalyst. *Acta Crystallogr. B.* **2014**, *70*, 498−509.
(30) De Smit, E.; Weckhuysen, B. M. The Renaissance of Iron-Based Fischer−Tropsch Synthesis: On the Multifaceted Catalyst Deactivation Behaviour. *Chem. Soc. Rev* **2008**, *37*, 2758.
(31) Bezemer, G. L.; Bitter, J. H.; Kuipers, H. P. C. E.; Oosterbeek, H.; Holewijn, J. E.; Xu, X.; Kapteijn, F.; Van Dillen, A. J.; De Jong, K. P. Cobalt Particle Size Effects in the Fischer−Tropsch Reaction Studied with Carbon Nanofiber Supported Catalysts. *J. Am. Chem. Soc.* **2006**, *128*, 3956−3964.
(32) Torres Galvis, H. M.; Bitter, J. H.; Davidian, T.; Ruitenbeek, M.; Dugulan, A. I.; De Jong, K. P. Iron Particle Size Effects for Direct Production of Lower Olefins from Synthesis Gas. *J. Am. Chem. Soc.* **2012**, *134*, 16207−16215.
(33) Casavola, M.; Hermannsdörfer, J.; De Jonge, N.; Dugulan, A. I.; De Jong, K. P. Fabrication of Fischer-Tropsch Catalysts by Deposition of Iron Nanocrystals on Carbon Nanotubes. *Adv. Funct. Mater.* **2015**, *25*, 5309−5319.
(34) Cheng, K.; Ordomsky, V. V.; Virginie, M.; Legras, B.; Chernavskii, P. A.; Kazak, V. O.; Cordier, C.; Paul, S.; Wang, Y.; Khodakov, A. Y. Support Effects in High Temperature Fischer-Tropsch Synthesis on Iron Catalysts. *Appl. Catal. A Gen.* **2014**, *488*, 66−77.
(35) Suo, H.; Wang, S.; Zhang, C.; Xu, J.; Wu, B.; Yang, Y.; Xiang, H.; Li, Y. W. Chemical and Structural Effects of Silica in Iron-Based Fischer-Tropsch Synthesis Catalysts. *J. Catal.* **2012**, *286*, 111−123.
(36) Park, J. Y.; Lee, Y. J.; Khanna, P. K.; Jun, K. W.; Bae, J. W.; Kim, Y. H. Alumina-Supported Iron Oxide Nanoparticles as Fischer−Tropsch Catalysts: Effect of Particle Size of Iron Oxide. *J. Mol. Catal A. Chem.* **2010**, *323*, 84−90.
(37) Perrichon, V.; Charcosset, H.; Barrault, J.; Forquy, C. Influence of a Partial Dissolution of Alumina during the Preparation of Iron Catalysts on Their Catalytic Properties for Fischer-Tropsch Synthesis. *Appl. Catal.* **1983**, *7*, 21−29.
(38) Wielers, A. F. H.; Kock, A. J. H. M.; Hop, C. E. C. A.; Geus, J. W.; Van Der Kraan, A. M. The Reduction Behavior of Silica-Supported and Alumina-Supported Iron Catalysts: A Mössbauer and Infrared Spectroscopic Study. *J. Catal.* **1989**, *117*, 1−18.
(39) Munnik, P.; Krans, N. A.; De Jongh, P. E.; De Jong, K. P. Effects of Drying Conditions on the Synthesis of $Co/SiO_2$and Co/Al_2O_3Fischer−Tropsch Catalysts. *ACS Catal.* **2014**, *4*, 3219−3226.
(40) Duvenhage, D. J.; Coville, N. J. $Fe:Co/TiO_2$ Bimetallic Catalysts for the Fischer-Tropsch Reaction: Part 2 The Effect of Calcination and Reduction Temperature. *Appl. Catal. A Gen* **2002**, *233*, 63−75.
(41) Oschatz, M.; Van Deelen, T. W.; Weber, J. L.; Lamme, W. S.; Wang, G.; Goderis, B.; Verkinderen, O.; Dugulan, A. I.; De Jong, K. P. Effects of Calcination and Activation Conditions on Ordered Mesoporous Carbon Supported Iron Catalysts for Production of Lower Olefins from Synthesis Gas. *Catal. Sci. Technol.* **2016**, *6*, 8464−8473.
(42) Meunier, F. C. Bridging the Gap between Surface Science and Industrial Catalysis. *ACS Nano* **2008**, *2*, 2441−2444.
(43) Van Deelen, T. W.; Nijhuis, J. J.; Krans, N. A.; Zečević, J.; De Jong, K. P. Preparation of Cobalt Nanocrystals Supported on Metal Oxides to Study Particle Growth in Fischer-Tropsch Catalysts. *ACS Catal.* **2018**, *8*, 10581−10589.
(44) Wolf, M.; Gibson, E. K.; Olivier, E. J.; Neethling, J. H.; Catlow, C. R. A.; Fischer, N.; Claeys, M. In-Depth Characterisation of Metal-Support Compounds in Spent Co / SiO 2 Fischer-Tropsch Model Catalysts. *Catal. Today* **2020**, *342*, 71−78.
(45) Casavola, M.; Xie, J.; Meeldijk, J. D.; Krans, N. A.; Goryachev, A.; Hofmann, J. P.; Dugulan, A. I.; De Jong, K. P. Promoted Iron Nanocrystals Obtained via Ligand Exchange as Active and Selective Catalysts for Synthesis Gas Conversion. *ACS Catal.* **2017**, *7*, 5121−5128.
(46) Krans, N. A.; Van der Feltz, E. C.; Xie, J.; Dugulan, I. A.; Zečević, J.; De Jong, K. P. Attachment of Iron Oxide Nanoparticles to Carbon Nanotubes and the Consequences for Catalysis. *ChemCatChem* **2018**, *10*, 3388−3391.
(47) Klencsár, Z. Mössbauer Spectrum Analysis by Evolution Algorithm. *Nucl. Instrum. Methods Phys. Res B* **1997**, *129*, 527−533.
(48) Wezendonk, T. A.; Santos, V. P.; Nasalevich, M. A.; Warringa, Q. S. E.; Dugulan, A. I.; Chojecki, A.; Koeken, A. C. J.; Ruitenbeek, M.; Meima, G.; Islam, H. U.; Sankar, G.; Makkee, M.; Kapteijn, F.; Gascon, J. Elucidating the Nature of Fe Species during Pyrolysis of the Fe-BTC MOF into Highly Active and Stable Fischer-Tropsch Catalysts. *ACS Catal.* **2016**, *6*, 3236−3247.
(49) Cheng, K.; Virginie, M.; Ordomsky, V. V.; Cordier, C.; Chernavskii, P. A.; Ivantsov, M. I.; Paul, S.; Wang, Y.; Khodakov, A. Y. Pore Size Effects in High-Temperature Fischer − Tropsch Synthesis over Supported Iron Catalysts. *J. Catal.* **2015**, *328*, 139−150.
(50) Ohtani, B.; Prieto-Mahaney, O. O.; Li, D.; Abe, R. What Is Degussa (Evonik) P25? Crystalline Composition Analysis, Reconstruction from Isolated Pure Particles and Photocatalytic Activity Test. *J. Photochem. Photobiol. A Chem* **2010**, *216*, 179−182.
(51) Torres Galvis, H. M.; Bitter, J. H.; Khare, C. B.; Ruitenbeek, M.; Dugulan, A. I.; de Jong, K. P. Supported Iron Nanoparticles as Catalysts for Sustainable Production of Lower Olefins. *Science* **2012**, *335*, 835−838.
(52) Gao, X.; Shen, J.; Hsia, Y.; Chen, Y. Reduction of Supported Iron Oxide Studied by Temperature-Programmed Reduction Combined with Mössbauer Spectroscopy and X-Ray Diffraction. *J. Chem. Soc., Faraday Trans.* **1993**, *89*, 1079−1084.
(53) Wolf, M.; Mutuma, B. K.; Coville, N. J.; Fischer, N.; Claeys, M. Role of CO in the Water-Induced Formation of Cobalt Oxide in a High Conversion Fischer−Tropsch Environment. *ACS Catal.* **2018**, *8*, 3985−3989.
(54) Litter, M. I.; Navío, J. A. Photocatalytic Properties of Iron-Doped Titania Semiconductors. *J. Photochem. Photobiol. A Chem* **1996**, *98*, 171−181.
(55) Kuipers, H. P. C. E. Quantitative Photoelectron Spectroscopy as Applied to Non-Ideal Surfaces. *Solid State Ionics* **1985**, *16*, 15−21.

https://dx.doi.org/10.1021/acs.chemmater.0c01352
Chem. Mater. 2020, 32, 5226−5235

(56) Kerkhof, F. P. J. M.; Moulijn, J. A. Quantitative Analysis of XPS Intensities for Supported Catalysts. *J Phys. Chem.* **1979**, *83*, 1612−1619.
(57) Craje, M. W. J.; Louwers, S. P. A.; De Beer, V. H. J.; Prins, R.; Van der Kraan, A. M. An EXAFS Study on the So-Called "Cobalt-Molybdenum-Sulfur" Phase in Cobalt/Carbon and Cobalt-Molybdenum/Carbon, Compared with a Moessbauer Emission Spectroscopy Study. *J. Phys. Chem.* **1992**, *96*, 5445−5452.
(58) McCammon, C. A.; Price, D. C. Mössbauer Spectra of Fe_xO (X>0.95). *Phys. Chem. Miner.* **1985**, *11*, 250−254.
(59) Bancroft, G. M. Mössbauer Spectroscopic Studies of the Chemical State of Iron in Silicate Minerals. *J. Phys. Colloques* **1979**, *40*, C2-464−C2-471.
(60) Santos, V. P.; Borges, L.; Sartipi, S.; van der Linden, B.; Dugulan, A. I.; Chojecki, A.; Davidian, T.; Ruitenbeek, M.; Meima, G. R.; Kapteijn, F.; Makkee, M.; Gascon, J. High-Temperature Fischer-Tropsch Synthesis over FeTi Mixed Oxide Model Catalysts: Tailoring Activity and Stability by Varying the Ti/Fe Ratio. *Appl. Catal. A-Gen.* **2017**, *533*, 38−48.
(61) Yu, S.; Zhang, T.; Xie, Y.; Wang, Q.; Gao, X.; Zhang, R.; Zhang, Y.; Su, H. Synthesis and Characterization of Iron-Based Catalyst on Mesoporous Titania for Photo-Thermal F-T Synthesis. *Int. J. Hydrogen Energy* **2015**, *40*, 870−877.
(62) Weller, M.; Overton, T.; Rourke, J.; Armstrong, F. *Inorg. Chem.* **2018**.
(63) Kim, W.; Moon, S. J.; Kim, C. S. Mössbauer Studies of Fe^{2+} and Fe^{3+} Mixed State in Ilmenite-Hematite Solid Solution. *Hyperfine Interact.* **2008**, *185*, 167−171.
(64) Shechter, H.; Hillman, P.; Ron, M. Mössbauer Study of the Structure and Decomposition of Wustite. *J. Appl. Phys.* **1966**, *37*, 3043−3047.
(65) Munnik, P.; Velthoen, M. E. Z.; De Jongh, P. E.; De Jong, K. P.; Gommes, C. J. Nanoparticle Growth in Supported Nickel Catalysts during Methanation Reaction—Larger is Better. *Angew. Chem. Int. Ed.* **2014**, *53*, 9493−9497.

https://dx.doi.org/10.1021/acs.chemmater.0c01352
Chem. Mater. 2020, 32, 5226−5235